INTERNATIONAL ATOMIC ENERGY AGENCY
UNITED NATIONS EDUCATIONAL, SCIENTIFIC AND CULTURAL ORGANIZATION
INTERNATIONAL CENTRE FOR THEORETICAL PHYSICS
I.C.T.P., P.O. BOX 586, 34100 TRIESTE, ITALY, CABLE: CENTRATOM TRIESTE

SMR.703 - 20

WORKING PARTY ON
MECHANICAL PROPERTIES OF INTERFACES

23 AUGUST - 3 SEPTEMBER 1993

"High Temperature Failure in Ceramics" (Part II)

"Stability and Surface Energies of Wetted Grain Boundaries in Aluminum Oxide"

Sheldon WIEDERHORN
United States Department of Commerce
National Institute of Standards and Technology
Materials Science and Engineering Laboratory
Building 233, Room B309
Gaithersburg, MD 20899
U.S.A.

Stability and Surface Energies of Wetted Grain Boundaries in Aluminum Oxide

Doh-Yeon Kim
Seoul National University
Seoul 151-742, Korea,

S.M. Wiederhorn, B.J. Hockey, C.A. Handwerker and J.E. Blendell,
National Institute of Standards and Technology
Gaithersburg, MD 20899

Journal of the American Ceramic Society, submitted

March 23, 1993

Stability and Surface Energies of Wetted Grain Boundaries in Aluminum Oxide

Doh-Yeon Kim
Seoul National University
Seoul 151-742, Korea,

S.M. Wiederhorn, B.J. Hockey, C.A. Handwerker and J.E. Blendell,
National Institute of Standards and Technology
Gaithersburg, MD 20899

Abstract

The stability of a calcium-aluminum-silicate liquid film between two near-basal plane surfaces of sapphire at 1650°C was studied. Samples were prepared having an average basal misorientation across the interface of 6-7° about $\langle 10\bar{1}0 \rangle$. The interfaces varied in orientation from 0 to ≈38° to the [0001] direction. Three types of interfaces were observed: faceted, solid-liquid interfaces; low-angle grain boundaries consisting of aligned arrays of dislocations; and boundaries consisting of alternating regions of dislocations and faceted solid-liquid interfaces. The type of interface observed depended on the orientation of the interface and could be predicted by using a construction based on Wulff shapes. Because the type of interface depends on crystal alignment and interface angle, these results suggest an absolute method of determining the surface free energy of wetted boundaries.

1. INTRODUCTION

Glass forming additives are often introduced to facilitate the processing of polycrystalline ceramics, and it is widely recognized that the physical behavior of these ceramics are controlled by a residual layer of glass at the grain boundaries. Changes in the sintering temperature, strength, toughness, creep rate, dielectric properties and many other properties have been directly attributed to the glass phase composition or morphology. Hence, grain boundary wetting by glass and the stability of thin glass layers at grain boundaries are important in ceramic science and technology and are subjects of continued interest to materials scientists.

Smith [1] proposed a simple thermodynamic criterion for grain boundary wetting based on the relative energies, per unit area, of the grain boundary, γ_{gb}, and the two solid-liquid interfaces, γ_{sl}, which replace the grain boundary on wetting: $2\gamma_{sl}<\gamma_{gb}$. All surface energies were assumed to be isotropic, but γ_{gb} could depend on the misorientation of the grains forming the grain boundary. Smith's work was expanded by others and extended to ceramics by Van Vlack [2] and by White [3].

One problem that has not been investigated is the role of surface energy anisotropy in the wetting process. Most crystalline minerals in contact with liquids exhibit planar facets. Crystals with anisotropic surface energy can facet to minimize their total surface free energy per unit volume. The limits implied by the simple wetting criterion of $2\gamma_{sl}<\gamma_{gb}$, still hold even if the solid-liquid surfaces are fully-faceted, but γ_{sl} and γ_{gb} must be modified to account for the anisotropy.

2. WETTING OF GRAIN BOUNDARIES

When a grain boundary of a given orientation is wetted, the resulting interface in a fully-faceted system will be composed of two faceted solid-liquid interfaces. The total solid-liquid surface energy is the sum of two different terms, γ_{sl}^{1} and γ_{sl}^{2}, one for each surface of the wetted grain boundary. Each of the γ_{sl}^{1} terms is a summation of the surface energies of the

facet planes for that orientation, each weighted by the area of the respective facet. If $\gamma_{sl}^1+\gamma_{sl}^2 < \gamma_{gb}$ for all interface orientations, then all interfaces will be wetted; if $\gamma_{sl}^1+\gamma_{sl}^2 > \gamma_{gb}$ for all interface orientations, the grain boundary will remain intact. Between these limits, the wetting of grain boundaries will depend on both the misorientation of the grains and the orientation of the interface normal. Since solid-liquid surface energies for a fully-faceted crystal differ from one orientation to the next, grain boundary segments in some interface orientations may wet readily, whereas boundary segments in other orientations may not wet at all. Thus, in a polycrystalline material a range of wetting behavior will be seen.

In this paper we explore the consequence of grain boundary plane orientation on the wetting of grain boundaries in a system which exhibits faceting of solid-liquid interfaces: aluminum oxide - anorthite ($CaAl_2Si_2O_8$). The alumina-anorthite is a good model for wetting in anisotropic systems. Faceting of interfaces between alumina and silicate-based liquids has been observed in many investigations [4-8] and some grain boundaries have been observed in polycrystals even when most grains are separated by liquid [9-10]. In aluminum oxide, the macroscopic equilibrium shape of isolated crystals in contact with liquid and liquid-filled pockets is a basal platelet bounded by (0001) facets and facets of off-basal orientations, including $(10\bar{1}2)$ and $(1\bar{2}13)$, depending on the silicate liquid composition. The equilibrium shape of a crystal in contact with liquid can be found from the shapes of isolated liquid-filled pockets. In polycrystalline alumina containing anorthite, solid-liquid interfaces break down into small-scale facets corresponding to the facets in the equilibrium shape, known as the Wulff shape.

Flaitz and Pask [9] and Shaw and Duncombe [10] found that when polycrystalline aluminum oxide is immersed in anorthite liquid presaturated with alumina, the liquid penetrates along most of the grain boundaries of the aluminum oxide. The alumina grains, which were initially equiaxed, become faceted as they are wetted by the liquid. The change in grain shape by faceting causes the grains to push apart. The sample volume increases and the

aluminum oxide grains appear to repel one another. In the final microstructure, most alumina grains are bounded by large-scale facets and are completely separated by thick layers of liquid; some grains remain bonded [10]. Phillips and Shiue [6] found similar results for commercial grades of vitreous bonded alumina; in which low-angle grain boundaries and basal twins are not penetrated by glass. These results are not unique to the alumina system, but occur in many systems which contain glass [11-13].

In this paper an experiment is described in which the wetting of grain boundaries can be easily explored, in a single experiment, over a wide range of interface normals for a given misorientation between grains initially separated by liquid anorthite. The low-angle grain boundary investigated here, a 7° tilt boundary, falls between the wetting limits described above. In this boundary, three types of equilibrium interface structures are observed. Depending on grain boundary normal orientation, the boundary may be entirely wetted by the glass; may be unwetted, consisting of aligned arrays of resolvable dislocations; or may be an alternating mixture of the two in proportions that depend on the boundary normal. These results are explained in terms of a geometric construction for wetting in anisotropic systems based on the Wulff shape. A major result of this work is that, for interface shapes, the absolute energies of all faceted surfaces can be obtained from two additional pieces of data: the Wulff shape of the solid in contact with the liquid and the energy of one interface in the system. In the case presented here the interfacial energy that is known is the grain boundary energy as calculated from the Reed-Shockley equation.

3. EXPERIMENTAL PROCEDURE

Grain boundaries were prepared from sapphire single crystals and tape-casted polycrystalline alumina containing anorthite glass. The green ceramic tape was sandwiched between two crystals of sapphire, and sintered at 1650°C, figure 1. The sapphire grew through the polycrystalline tape to yield a structure consisting of two large single crystals separated by a liquid film

of glass. This procedure has the advantage over traditional grain growth geometries in that the sapphire-glass interface eventually becomes approximately stationary. Interface motion slows as the grains in the polycrystalline tape disappear, so that continued interface motion is less likely to affect the microstructure of the boundary. After the two sapphire crystals have grown together the boundary was wavy because growth is not uniform along the growth front [7]. As long range diffusion is required for the grain boundary to become truly flat, the local structure along the boundary will approach thermodynamic equilibrium much more rapidly than the boundary as a whole. Consequently, we assume that features we observe along the sapphire-glass interface are equilibrium features.

The average diameter and thickness of sapphire discs used were 13 mm and 2 mm, respectively. In all experiments, the c-axis was at an angle of ≈3.5° to the faces of the discs. For each experiment, a sapphire disc was polished on both sides and then cut along its diameter; these two pieces formed the two halves of the bicrystal. From TEM analysis, the misorientation between the two halves corresponds approximately to a 6°-7° tilt about a $\langle 10\bar{1}0 \rangle$ axis.

The alumina tape was produced by standard tape casting techniques using a commercial binder (Metoramic Sciences, Inc. Binder B73181)[1]. The alumina was a tabular alumina (Fujimi Abrasives) with an average particle size of approximately 15 μm. Anorthite ($CaAl_2Si_2O_8$) powder was prepared by first melting stoichiometric mixtures of CaO, Al_2O_3 and SiO_2. The melt was quenched and the resultant glass ground into a powder. The fraction of anorthite in the tape was 4 % by weight. The thickness of the green tape was 200 μm.

Specimens were hot-pressed in air with the stress axis perpendicular to the disk surfaces, as indicated in figure 1. To remove the organics used in tape-casting, the specimens were held at 600°C for one hour, then heated to 1000°C for one hour; the heating and cooling rates were 10°C/min. The specimens were then hot-pressed at 1650°C for 2 h under 7 MPa with no die wall

---

[1] The use of commercial designations does not imply endorsement by the National Institute of Standards and Technology.

constraint. The specimens were sectioned into several pieces perpendicular to the interface, so that each piece contained a layer of polycrystalline alumina/anorthite between the surfaces of the sapphire single crystals. One group of specimens was subsequently heat treated without load at 1600°C for various times up to 60 h in air. Another group was treated at the same temperature but under a uniaxial pressure of 10 MPa with the stress axis perpendicular to the disc surface. The microstructures of the heat-treated specimens were examined by optical microscopy. Specimens for transmission electron microscopy (TEM) were made by ultrasonic cutting followed by ion milling. All sections had the bicrystal interface approximately perpendicular to the TEM section.

4. EXPERIMENTAL RESULTS

Optical Microscopy - The microstructure of a hot-pressed specimen (1650°C, 7 Mpa, 2 h) is shown in figure 2. It consists of a layer of polycrystalline alumina sandwiched between two single crystals of sapphire. Almost all of the grain boundaries seem to be wetted by anorthite glass, even at this low magnification. This finding is consistent with earlier TEM studies on this type of structure [4-8]. Pockets of glass are located at triple junctions. The original interface between the sapphire and the tape is marked by a planar array of pores trapped in the sapphire by the advancing sapphire boundary. The migration rate of the sapphire is not uniform, resulting in an interface that is not flat. Slow dissolution of relatively large grains with basal plans normal to the advancing front appear to be the main cause of such nonuniform migration. This observation is consistent with earlier studies of grain growth in vitreous bonded alumina [7, 15]. Both growth and dissolution in the ‹0001› occur more slowly than planes of other crystallographic orientations.

In figure 3 we show a sequence of photomicrographs illustrating sapphire boundary migration as a consequence of heat treatment at 1600°C. Cavities that are left behind in the sapphire by the advancing boundary normally

contain anorthite glass. This observation and the fact that glass does not build up at the sapphire-tape interface suggests entrapment of glass by the migration process. Entrapped pockets of glass behind the moving sapphire front have, in fact, been reported earlier [7]. After 10 h of annealing, figure 3a, most of the alumina grains within the tape have disappeared; only a single layer remains. Some alumina grains in this layer form grain boundaries, both with each other and with the sapphire crystals. The sapphire interfaces remain irregular, a consequence of the irregular advance of the sapphire through the alumina tape.

Annealing for 20 h at 1600°C completely eliminates all grains of the alumina tape, figure 3b. A thin layer of anorthite glass now separates the two single crystals of sapphire. The sapphire-glass interface is microscopically non-planar, with facets visible by optical microscopy. In some regions, contact between the sapphire crystals was observed at this stage of annealing. The glass layer varied in apparent thickness from zero to 2.5 μm.

An additional heat treatment of 40 h at 1600°C (60 h total), figure 3c, illustrates the growth of junctions between the sapphire crystals. At many points along the sapphire-anorthite interfaces, the sapphire crystals appear to be in contact. As will be shown, contact depends on the local interface normal. Further heat-treatment, up to 60 h (120 h total), produced no additional changes in the interface microstructure.

To accelerate the formation of the bicrystal, a compressive stress of 10 MPa was applied during heat-treatment. Application of pressure increased the rate of interface migration, figure 4. The aluminum oxide grains in the tape have completely disappeared and there are large areas of contact between the sapphire disks after only 10 h at 1600°C, as compared with 40 h without an applied load. Optical microscopy indicates that the fraction of apparent contact is larger and the remnant glass layer is thinner in the samples annealed under load. As with the stress-free sintered material, the boundary is not flat and most of the glass appears to have been entrapped within the

sapphire crystals. Further details of the interface cannot be resolved by optical methods.

Transmission Electron Microscopy - Transmission Electron Microscopy (TEM) observations were made exclusively on samples produced by pressure sintering, as the frequency of interface contact was greater in these samples. All observations were made on <10$\bar{1}$0> oriented cross-section foils which necessarily contain the normal direction of migration. Moreover, as determined by subsequent diffraction analysis, the specific [10$\bar{1}$0] normal to the foils coincided with the major axis of rotation describing the orientation of the two sapphire crystals[2]. From this prospective, microstructural details of a pressure-sintered interface are shown in Figures 5-8.

Figure 5 provides a low magnification view of a large segment of the interface, which again illustrates that the interface is not flat and normal to the direction of crystal growth (vertical in Figure 5). Instead, the interface contains relatively large segments over which the local interface normal deviates from the direction of crystal growth, i.e. the mean interface normal[3], by approximately 38°, as in Figure 5.

In addition, image contrast, denoting a change in the structure of the interface, can be seen to depend on the deviation of the local interface normal to the mean interface normal. In the upper right of Figure 5, where the interface normal is close to the mean interface normal, the opposing sapphire surfaces are faceted and clearly separated by a glassy interphase. In contrast, the left side of the interface, where the interface normal is ≈38° from the mean interface normal, is marked by image contrast characteristic of an array of dislocations edge on to the foil (i.e., along [10$\bar{1}$0]). Finally, within the intervening region, where the interface normal

---

[2] The misorientation also contained smaller rotation components about the median [0001]; these, however, resulted in less than a 3° misorientation between the [10$\bar{1}$0] of the two crystals, and are ignored.

[3] The mean interface normal is defined here as the normal to the original sapphire disc surfaces, i.e., effectively the crystal growth direction. At any point on the interface, the local normal can differ from the mean normal because of the uneven growth process.

is roughly 10° from the mean interface normal, both dislocation contrast and small, isolated, and faceted pockets of glass are seen. As will be shown in greater detail, these three characteristic regions correspond to three different types of boundaries, namely: fully-wetted boundaries; partially-wetted boundaries; and, non-wetted, low-angle grain boundaries.

Fully-wetted boundaries between the sapphire crystals are only observed for interface orientations that deviate approximately ± 3.5° from the mean interface normal. As illustrated in Figure 6, these interfaces are characterized by a glassy interphase of variable thickness. Also, the bounding sapphire surfaces are invariably faceted, with the nature of faceting being dependent on the local interface orientation. This change in facet structure with orientation is particularly evident in Figure 6a, where the change in interface orientation can be described by a small rotation about the common [10$\bar{1}$0] axis. Along the right hand side, the upper portion of the interface is planar along the (0001) basal plane of the upper crystal, whereas, the lower portion consists of (0001) and (1$\bar{2}$13) facets, relative to the lower crystal. Along the left hand portion, the interface structure is reversed commensurate with the relative change in interface orientation. Figure 6b, in which lattice fringes corresponding to the (0003) reflections in both crystal halves are imaged, shows that this description of fully-wetted interfaces applies even when the dimensions of the facet step heights and glass interphase thickness are comparable to the unit cell size of Al_2O_3. Here it can be noted that the orientation of the interface in Figure 6b is close to that for the left hand portion seen in Figure 6a. Except for the difference in scale, the interface structures are similar. Moreover, composition analyses of both interfaces indicated the presence of a glassy layer with a average composition corresponding to anorthite. For the interface seen in Figure 6a, comparative EDS results from regions containing the interface, from regions within large scale glass-filled pockets in this sample, and from an anorthite glass standard all showed similar Ca to Si peak intensity ratios. For the boundary in Figure 6b, a similar comparative

analysis by PEELS was used to obtain the concentration of Ca within a specified region containing the interface.[4] Assuming a glass layer with the composition of anorthite, this result led to a calculated value of ≈0.5 nm for the interface thickness, which is in reasonable agreement with the high resolution image, Figure 6b.

At the other extreme, fully-dewetted interfaces are only observed when the deviation angle between the local interface normal and mean interface normal was large, roughly 38°, with 42° being the largest angle of deviation observed. As illustrated at the left side of Figure 5, these interfaces exhibit dislocation image contrast, suggesting they are low-angle grain boundaries and, therefore, free of residual glass. This interpretation is strengthened by high resolution observations of the interface, Figure 7, and by PEELS analysis, which showed no evidence of Ca (within the detection limit) at the interface. In Figure 7, the interface is seen under conditions where the [0003] reflections in both crystals are strongly reflecting.

At the interface, which is marked by residual strain contrast, there is an abrupt change in fringe direction, defining a 7° misorientation (about $[10\bar{1}0]$) of the two crystals. Close inspection of Figure 7 shows that, while most fringes are continuous (although severely bent) at the interface, roughly one out of seven or eight fringes in the upper crystal terminates at the interface, indicating the presence of a 1/3[0001] partial dislocation or a dislocation having a Burgers vector with a 1/3[0001] component along c=[0001]. Here, it should be noted that, for the average (0003) fringe misregistry of one out of every ≈7.5 fringes, the misregistry is only slightly larger than that obtained from either simple geometric consideration or the application of Frank's analysis [16] (assuming the presence of individual $1/3[1\bar{2}10]$ and 1/3[0001] dislocations), both of which predict misregistry at every six [0003] fringes for this tilt boundary.

---

[4] For Al_2O_3-anorthite, quantifiable results by PEELS at the ppm levels could only be obtained for Ca. This analysis was performed on a VG STEM (HB501) microscope.

For intermediate angles of deviation, $\approx 3.5 < \Phi < 38°$, the interface is found to be composed of fully-wetted and fully-dewetted segments and can be described as a partially-wetted boundary. As before, this description applies regardless of scale, as illustrated in Figure 8. In Figure 8a, the angle of deviation of the local interface normal (measured over ≈5μm) from the mean interface normal is about 13°. Within this relatively large angular range, the interface is seen to contain large faceted pockets of glass (fully-wetted) connected by planar boundary segments. The boundaries were found (by diffraction contrast and PEELS analyses) to correspond to low-angle dislocation boundaries (fully-dewetted). Figure 8b shows a portion of the interface at higher resolution. Here, [0003] lattice fringe imaging indicates the presence of faceted glass pockets of interplanar dimensions separated by regions over which the fringes are continuous, except at the sites of dislocations, similar to Figure 7. The presence of glass at this partially-dewetted interface was again supported by PEELS analysis, which showed a detectible concentration of Ca within the interface.

5. DISCUSSION OF RESULTS

This study illustrates the diverse nature of grain boundaries in aluminum oxide in the presence of a liquid phase. Depending on the angle of the boundary normal to the mean interface normal, fully-wetted boundaries, unwetted boundaries or a combination of the two were obtained. These observations can be explained by comparing energies of unwetted grain boundaries with those of wetted crystal surfaces. The unwetted boundaries are assumed to be low-angle grain boundaries in which the energy is determined by the sum of the core energy and the elastic energy of the dislocations that make up the boundary. The energy of the wetted boundary is determined from the energy of the two faceted and wetted surfaces. The relative energies of the faceted interfaces can be found if the equilibrium shape of the crystal is known, i.e. if the Wulff shape is known. A model of the energy of the wetted

boundary (based on Herring's construction for the energy of a faceted surface [14]) is used to explain our data.

Nominally, 5 angles of orientation are required to define an arbitrary grain boundary between two crystals: three for the relative orientation of the two crystals and two for the orientation of the boundary between the crystals. In the present study, two of the angles defining the relative orientation of the two crystals are known since the [10$\bar{1}$0] is a common axis of the two crystals. The remaining angle of rotation between the two crystals is given by the tilt angle of the two crystals. Of the two angles defining the boundary normal, only one is observed in our experiment. In the discussion below, we define the tilt angle between the two crystals as Θ and the angle between the boundary normal and the mean interface normal as Φ. This geometry permits us to use a two-dimensional analysis to explain our experimental observations.

In this section we first calculate the energy of a grain boundary, γ_{gb}, as a function of tilt angle Θ and grain boundary orientation Φ. The surface energy, γ_{s1}^1 and γ_{s1}^2, of the two interfaces that make up the wetted boundary is then calculated from the Wulff shape, using the Herring [14] method of spheres. Finally, we obtain the energy and shape of the stable interface by comparing the energy of the wetted boundary, $\gamma_{s1}^1 + \gamma_{s1}^2$, to the energy of the grain boundary γ_{gb}. Theoretical predictions of stable structures are consistent with our experimental observations.

Grain Boundary Energy - The energy of the unwetted bicrystal boundary as a function of Θ and Φ can be estimated from the Reed-Shockley equation [17, 18]. The grain boundary energy is assumed to be equal to the sum of the core energy and elastic energy of dislocations in the grain boundary. Based on this theory, the energy of a boundary with two degrees of freedom, is given by the following equation [17]:

$$\gamma_{gb} = \gamma_{gb}^{\circ}(\Phi) \cdot \Theta \cdot [A(\Phi) - \ln \Theta] \qquad (1)$$

where Θ is the tilt angle between the two crystals, and γ_{gb}° and A are functions of Φ, the orientation of grain boundary. γ_{gb}° is also a function of

the shear modulus, Poisson's ratio and the Burgers vector, while ***A*** is a function of the core energy of the dislocations [17, 19]. For alumina, ***A*** was evaluated assuming that the ratio of the Burgers vector of the dislocations to the core radius is equal to ≈3 [19]. γ_{gb}^{o} was calculated from the elastic constants of aluminum oxide and the Burgers vector of the dislocations of the boundary. For purposes of this calculation, aluminum oxide was assumed to be elastically isotropic, with E = 380.0 GPa and ν = 0.24 [20], and a Burgers vector, b = 0.475 nm (= $1/3a_o$) [21].

Based on the above assumptions, the grain boundary energy of the bicrystal was calculated, figure 9. For low-angle boundaries γ_{gb} is more sensitive to the misorientation between the crystals, Θ, than to the angle of the grain boundary normal, Φ. For small misorientations, $\Theta<7°$, γ_{gb} is insensitive to the angle of the boundary normal. For this reason, we assume that for a fixed misorientation, Θ, γ_{gb} is not dependent on the orientation of the grain boundary. Thus γ_{gb} as a function of Φ is a circle and the Wulff shape is also a circle. We recognize that all materials exhibit some degree of anisotropy in γ_{gb} and that the Reed-Shockley theory may be too simple. Recent calculations [22] of the energy of low-angle grain boundaries predict an anisotropic γ_{gb}, leading to a faceted Wulff shape. However, the Reed-Shockley theory gives a reasonable first-order approximation to the grain boundary energy.

Energy of a Wetted Interface - To calculate the energy of a wetted interface in a sapphire bicrystal, we extend a construction developed to analyze the energy of faceted crystalline surfaces [14]. At equilibrium, crystals that facet are bounded by flat, low energy crystallographic planes that form the Wulff shape. Classically, the Wulff shape is constructed from the surface energy as a function of orientation by the Wulff construction [23, 24]. However, only for crystals which do not facet can the surface energy as a function of orientation be determined experimentally for all orientations. For any orientation that is not present in the Wulff shape, the surface energy of that orientation cannot be measured. What can be determined from a faceted

Wulff shape is the minimum surface energy as a function of orientation consistent with the shape, and it can be shown [14] that this minimum energy is the energy of the faceted surfaces themselves as a function of orientation. It is this minimum energy function that is relevant to whether or not wetting will occur. Thus, the energy of the faceted surfaces as a function of orientation can be determined experimentally from the equilibrium shapes of isolated liquid-filled pores, which give the relative energies of the facet planes, and the energy of any one surface which set the energy scale.

A two dimensional section of a crystal shape based on observed facets in Al_2O_3 is shown in figure 10a. The distances, l_i, from the origin to the crystal surfaces are proportional to the surface energy of those surfaces, γ_i, in such a way that γ_i/l_i is a constant. In figure 10a, the surfaces were selected to model the kinds of facets observed in our TEM experiments. The basal surface, (0001), is normal to the ordinate, whereas the pyramidal surface, $(1\bar{2}13)$, lies at an angle of 61° to the ordinate and it is assumed that $\gamma_{1\bar{2}13} = 1.4 \cdot \gamma_{0001}$ for this figure.

If a flat plane is polished at some arbitrary crystal orientation and permitted to come to equilibrium, it will facet into a set of low energy surfaces, thereby increasing the total surface area [14]. The surface energy per unit area of original polished surface is the sum of the specific surface energies of the facets (weighted by their areas). In two dimensions, the energy of the faceted surface is given by a circle that passes through the origin of the Wulff shape, through the corner where two crystal facets meet, and through both crystal facets at the normals[5] of the Wulff shape, figure 10a [14]. The vector, σ, from the origin to the corner is the hypotenuse of an inscribed right angle triangle, and thus it is the diameter of the circle. This diameter vector completely characterizes the size and position of the circle, and, hence, the energy of the faceted surface.

---

[5] In figure 10b, the crystal facet normal lies on the crystal surface, although it can lie on an extension of the crystal surface.

For any given surface orientation with unit normal, $\mathbf{n}$, the surface energy, γ, is: $\gamma=\mathbf{n}\cdot\sigma$ [14], which is the equation of a circle through the origin. Thus, all that is needed to define the surface energy of a random plane is the set of diameter vectors, $\{\sigma\}$. These are all contained in the Wulff shape.

Two types of circles can be drawn in figure 10a, one type going through corners labeled A (as shown in the figure), the other type going through corners labeled B. These circles also pass through the adjacent crystal facet normals and the origin. Each circle intersects a neighboring circle at the crystal facet normal. The outer envelope of circles constructed in this manner, i.e. in a manner determined from the Wulff shape, have physical reality in that the distance from the origin to the circle represents the energy per unit area of faceted surface of that orientation. The outer envelope of the construction is given in figure 10b.

Shape of a Wetted Bicrystal Boundary - It should be noted that, at this point, the Wulff shape has no energy scale. Only the relative energies are known from the shapes of isolated crystals or liquid-filled pockets. In order to have an energy scale for the Wulff shape, the energy of any one interface must be known. It is important to remember that in this section on the wetted bicrystal boundary, the energies are only relative energies. The absolute energy scale is provided in the following section on the combined surface energy diagram.

In the current experiment, the wetted bicrystal boundary energy can be found using the interfacial energies of both faceted solid-liquid surfaces such as that depicted in figure 10b. There are a number of mathematically equivalent constructions for the boundary energy, one of which is presented here. An alternate construction is given in appendix A. As the crystals that make up the boundary are tilted relative to each other, the energy of the two halves of the wetted boundary at any orientation will come from slightly different portions of the surface energy curve of the two crystals. This situation is shown in figure 11. In this diagram each surface energy curve is

tilted with respect to the ordinate, which represents the mean interface normal of the two crystals. One crystal is tilted at +3.5°, the other at -3.5°. To obtain the surface energy of the wetted bicrystal interface, the surface energies of each crystal are added together for each value of interface orientation, Φ. This gives the energy for the fully-wetted and faceted boundary as a function of orientation, and is shown in figure 12. Also shown in figure 12 is the (macroscopic) shape of the fully-wetted interface, which is found by using the Wulff construction.[6] This bicrystal Wulff construction gives the Wulff shape for the wetted faceted bicrystal, W_c, and will be used to estimate the energy of partially-wetted boundaries. In two dimensions, there is one facet in the combined shape for each of the facets in the single crystals.[7]

The distance from the origin to each facet of the combined shape gives the energy of the bicrystal "facet". As in the case of the Wulff shape for a single crystal, the energy of any wetted bicrystal surface is given by: $\gamma = \mathbf{n}\cdot\boldsymbol{\sigma}$, where $\boldsymbol{\sigma}$ is the vector from the origin to the corner of the combined Wulff shape. Thus, all that is needed to define the energy of the wetted faceted interface is the bicrystal Wulff shape.

This combined shape, W_c, is the macroscopic shape which a crystal, inside another crystal and misoriented by Θ, would assume for a fully-wetted interface. At the macroscopic level it contains faceted interfaces, but at higher magnifications the shape of the interface is much more complicated as shown in figures 5-8. The structure of a wetted bicrystal boundary is determined by the orientation of the boundary normal. The two faceted solid-liquid interfaces of the bicrystal boundary have to be consistent with the faceting which occurs at that orientation on the surface of the crystals that

---

[6] As with the single crystal, a line perpendicular to γ_i for each Φ is constructed. The inner envelope of such a collection of lines defines the Wulff shape for the combined interface. The sides are given by the facets of the original crystals, rotated with respect to each other by Θ.

[7] In three dimensions additional surfaces show up. These are discussed in detail by Carter et al. [25].

make up the boundary. For most orientations, both surfaces of the boundary are faceted. However, at special orientations, indicated by cusps in the combined energy diagram, the boundary orientation is such that one surface of the boundary lies normal to a facet plane in that crystal and will be flat in the wetted interface. These orientations are determined by the original Wulff shape. The kind of interface structures expected are also illustrated in figure 12. These are the structures which are observed in the current experiments, figure 5. At +3.5° or -3.5° the boundary consists of a basal surface on one side and a faceted surface consisting of basal and pyramidal planes on the other. Between the two orientations, both surfaces are faceted. The same sort of argument holds true at each of the cusps shown in figure 12.

Combined Surface Energy Diagram - There are several equivalent methods for determining interfacial structural stability of boundaries in crystals [26]. In this section, we present a method that is based on combined Wulff shapes for the stable interfaces present in the system. If the Wulff shape of an unwetted, low-angle grain boundary is superimposed on the Wulff shape of a fully-wetted, figure 13a, then the inner envelope of the two shapes is the Wulff shape of the stable interface, Figure 13b. This figure can be used to construct the minimum energy surface for the interface. Because γ_{gb} is assumed to be independent of the grain boundary orientation angle, Φ, the grain boundary Wulff shape appears as a circle on the figure. The two shapes are scaled so that the Wulff shape for the grain boundary cuts W_c at an angle of 38° to the vertical axis. Therefore, it follows that the energy of the wetted boundary is known relative to the energy of the low angle grain boundary. This angle of 38° is selected because it corresponds to the interface normal beyond which only grain boundaries are stable in our experiments.

The surface energy of the combined interface is obtained by the same method as that used to determine the energy of faceted surfaces from the Wulff plot for a single crystal. Diameter vectors are drawn from the origin to the

corners of the Wulff shape. The outer envelope of circles generated from these vectors yields the energy of the combined boundary, figure 13c.

The circles that make up the energy surface in figure 13c have three different sizes. Between -3.5° and 3.5°, the diameter vector is identical to that used to construct the energy surface for the wetted boundary. Hence, for this range of angles, a fully wetted boundary is expected. For angles between 38° and 128°, the energy surface is identical to the surface of the unwetted grain boundary. Therefore, unwetted low angle grain boundaries are expected for this range of angles.

For angles between 3.5° and 38°, the energy surface is congruent with neither the wetted nor the unwetted energy surfaces. This portion of the energy surface represents a partially wetted surface consisting of wetted segments and unwetted grain boundaries. The wetted segments have the structure typical of wetted boundaries at ±3.5°. The energy of this portion of the energy surface is given by the sum of the energies from the wetted and unwetted segments of the boundary, weighted by their respective areas.

Examination of the microstructures of partially-wetted boundaries indicates that the predictions of the structure as a function of interface normal are largely satisfied. Between orientations of 3.5° and -3.5° fully-wetted boundaries are indeed observed, figure 7, and the faceted appearance of these boundaries is as expected from theory. From 3.5° to approximately 38° structures with alternating grain boundaries and wetted boundaries are observed, figure 8; and for angles greater than 38°, low-angle grain boundaries are observed, figure 9. A closer examination, however, indicates a discrepancy between theory and experiment. From the two-dimensional analysis in figure 12, the cavities in the partially-wetted boundaries should be triangular; one side of the cavity should not have any facets. Thus, while the general trend of the data is in agreement with the theory, a small, but significant deviation between theory in 2-D and experiment is observed. We believe this deviation to be a consequence of using a two-dimensional theory for what is really a three-dimensional problem. In 3-D there are regions of

the shape in which two facets coexist on both sides of the interface. The various structures in 3-D will be explored in future studies.

Absolute Determination of Surface Energies - The magnitude of the surface energy curve of the fully-wetted boundary, figure 12, cannot be determined solely from the observed Wulff shapes. Only the relative values of the energies can be determined in this manner. An absolute value of the energy of at least one of the facets is normally needed to determine all of the other surface energies. In the present study, this absolute value of surface energy is determined from the theoretical estimate for the energy of the low angle grain boundaries. Since the energy of the low angle grain boundary and the wetted boundary Wulff shapes have been scaled to one another, figure 13, the absolute value of the wetted boundary can be determined, and from that the surface energies of the individual interfaces.

The data presented in this paper can be used to estimate the interface energy at 3.5°. From the interface energy, the surface energy of the basal plane, γ_{0001} can be obtained. The energy of the partially-wetted boundary at any Φ between 3.5° (the orientation of the cusp) and 38° is: $\gamma = \mathbf{n}\cdot\boldsymbol{\sigma}$, where n is the unit normal vector to the boundary and σ is the vector from the origin to the energy surface at 38°. As Φ varies between these angles, the fraction of glass pockets and grain boundary segments changes, but the shape of the glass-filled pockets and the orientation of the grain boundary does not change. At the cusp in the energy curve (Φ = 3.5°), $\mathbf{n}\cdot\boldsymbol{\sigma} = 2.3\cdot\cos(34.5°) = \gamma = 1.9$ J/m^2. Since the angle between the facets are fixed, the areas of the facets of the glass-filled pockets can be calculated. As the angle between the two basal planes is approximately 7°, the total area of wetted basal plane for a unit area of interface at Φ = 3.5° will be 1.91 m^2 while the area of the $(1\bar{2}13)$ plane will be 0.14 m^2. The specific surface energy of the pocket is the sum of the individual facet surface energies times their area:

$$\gamma_{pocket} = \mathbf{n}\cdot\boldsymbol{\sigma} = A_{0001}\gamma_{0001} + A_{1\bar{2}13}\gamma_{1\bar{2}13}. \qquad (2)$$

As all the facets we observe in these experiments are composed of either a single basal facet or a combination of a basal and a pyramidal facet, and

none are only a pyramidal facet, there is a lower limit of the surface energy ratio, $R = \gamma_{1\bar{2}13}/\gamma_{0001} = 1.1$ in order to have the corner of W_c at an angle greater than 38°. For $R = 1.1$, $\gamma_{0001} = 0.91$ J/m^2 and $\gamma_{1\bar{2}13} = 1.0$ J/m^2. As R increases, γ_{0001} decreases. Based on our observations of the shape of pores in sapphire [27], $R < 2$. Assuming the same value of R for glass filled pores, $\gamma_{0001} > .86$ J/m^2 and $\gamma_{1\bar{2}13} < 1.7$ J/m^2. Although a better experimental determination of R is needed for a more accurate value of γ_{0001}, the above discussion does illustrate a method by which the surface energies of wetted facet planes can be determined.

6. SUMMARY

An investigation of the stability of liquid films between sapphire crystals with near-basal orientations was conducted. Dewetting of the interfaces was found to depend on the crystal misalignment, Θ, and interface orientation, Φ. For a simple 6°-7° tilt boundary about the [10$\bar{1}$0] axis, three types of boundaries were observed. For small angles of Φ, -3.5° to 3.5°, fully-wetted, faceted surfaces were observed. These were composed of a mixture of basal and pyramidal planes. For angles, Φ, between 3.5° and approximately 38°, the boundary was partially-wetted, consisting of low-angle grain boundaries and glass-filled, faceted cavities bounded by basal and pyramidal planes. For angles greater than 38° only low-angle grain boundaries were observed. These observations could be explained through a construction comparing the energy of a grain boundary to the energy of a wetted, faceted boundary. In this construction, all three types of structures are predicted. Using a calculated value of the energy of a 7° tilt grain boundary as a scaling parameter, the specific surface energy of a fully-wetted faceted bicrystal boundary at $\Phi = 3.5°$ is ≈ 1.9 J/m^2. Assuming $\gamma_{1\bar{2}13}/\gamma_{0001} = 1.1$, the specific surface energy of the basal surface is found to be: $\gamma_{0001} \approx 0.9$ J/m^2.

ACKNOWLEDGEMENT

The financial support of the Office of Naval Research is gratefully acknowledged. The STEM/PEELS analysis was performed at the National Institutes of Health with the assistance of Richard Leapman. The assistance of Yigal Finkelstein and Terry Baker in the early stages of this work was invaluable. Critical discussions with John Cahn and Craig Carter are gratefully acknowledged.

APPENDIX A

The Wulff shape for the wetted, faceted bicrystal boundary can be obtained in a simple manner directly from the Wulff shape of the wetted single crystal. The construction is illustrated in figure A1. The energy of the wetted, faceted bicrystal boundary is evaluated by adding the energies of the two wetted surfaces that make up the bicrystal. In figure 11, two surface energy curves are shown, one tilted at 3.5° to the axis, the other tilted at -3.5° to the axis. At a given angle, Φ, from the mean interface normal, the surface energies of each crystal are added to give the bicrystal surface energy. In effect, segments of circles from each of the single crystal surfaces energy curve are added to give the energy of the bicrystal surface energy. It can be shown that adding circles in this manner is equivalent to vectorially adding the diameters of the circles to yield the diameter of a new circle that represents the surface energy of the bicrystal boundary. These diameter vectors also represent the corners of the combined Wulff shape, so that the Wulff shape for the wetted, faceted bicrystal boundary is obtained by adding the diameter vectors that go to the corners of the Wulff shape of the individual crystals that make up the boundary. In the case studied here, the diameter vectors to be added can be selected by inspection. This process is illustrated in figure A1 where diameter vectors from the primed and unprimed Wulff shapes from figure 11 are added to yield the combined Wulff shape. The combined Wulff shape is a 12-sided figure, with each face coming from the two rotated single-crystal Wulff shapes.

REFERENCES

1. C.S. Smith, "Some Elementary Principles of Polycrystalline Microstructure," Met. Rev., 9, 1-15 (1964).

2. L.H. Van Vlack, "Microstructure of Silica in the Presence of Iron Oxide," J. Am. Ceram. Soc. 43 [3] 140-145 (1960).

3. J. White, "The Nature of the Factors Determining the Structure of Polyphase Ceramics," pp. 305-30 in Science of Ceramics, Vol. 2, Edited by G.H. Stewart, Academic Press, London, 1965.

4. C.A. Powell-Dogan and A.H. Heuer, "Microstructure of 96% Alumina Ceramics: I, Characterization of the As-Sintered Materials," J. Am. Ceram. Soc., 72 [12] 3670-76 (1990).

5. S.C. Hansen and D.S. Phillips, "Grain-Boundary Microstructures in a Liquid-Phase Sintered Alumina (α-Al_2O_3)," Philos. Mag. A., 47, 209-34 (1983).

6. D.S. Phillips and Y.R. Shiue, "Grain-Boundary Microstructures in Alumina Ceramics," pp. 357-367 in Advances in Ceramics, vol. 10, *Structure and Properties of MgO and Al_2O_3 Ceramics*, W.D. Kingery Ed., The American Ceramic Society Inc., Columbus, OH (1984).

7. Y. Finkelstein, S.M. Wiederhorn, B.J. Hockey, C.A. Handwerker and J.E. Blendell, "Migration of Sapphire Interfaces into Vitreous Bonded Aluminum Oxide," pp. 258-279 in Ceramic Trans, vol. 7, *Sintering of Advanced Ceramics*, C.A. Handwerker, J.E. Blendell and W.A. Kaysser, Eds. The American Ceramic Society, Inc., Westerville, OH (1990).

8. Y.K. Simpson and C.B. Carter, "Faceting Behavior of Alumina in the Presence of a Glass," J. Am. Ceram. Soc., 73 [8] 2391-98 (1990).

9. P.L. Flaitz and J.A. Pask, "Penetration of Polycrystalline Alumina by Glass at High Temperatures," J. Am. Ceram. Soc. 70 [7] 449-55 (1987).

10. T.M. Shaw and P.R. Duncombe, "Forces between Aluminum Oxide Grains in a Silicate Melt and their Effect on Grain Boundary Wetting," J. Amer. Ceram. Soc. 74 [10] 2495-505 (1991).

11. D.R. Clarke, "On the Equilibrium Thickness of Intergranular Glass Phases in Ceramic Materials," J. Amer. Ceram. Soc. 70 [1] 15-22 (1987).

12. D.R. Clarke, "Grain Boundaries in Polycrystalline Ceramics," Ann. Rev. Mater. Sci. 17 57-74 (1987).

13. D.R. Clarke, "Intergranular Phases in Polycrystalline Ceramics," pp. 57-79 in *Surfaces and Interfaces of Ceramic Materials*, L.-C. Dufour et al. (eds.), Kluwer Academic Publishers (1989).

14. C. Herring, "Some Theorems on the Free Energies of Crystal Surfaces," Phys. Rev. 82 [1] 87-93 (1951).

15. W.A. Kaysser, M. Sprissler, C.A. Handwerker and J.E. Blendell, "Effect of a Liquid Phase on the Morphology of Grain Growth in Alumina," J. Am Ceram. Soc. 70 [5] 339-343 (1987).

16. F.C. Frank, Symposium on the Plastic Deformation of Crystalline Solids. pp 150 (1950).

17. W.T. Read, Jr., "Dislocations in Crystals," McGraw-Hill, New York, (1953)

18. W.T. Read, Jr. and W. Shockley, "Dislocation Models of Crystal Grain Boundaries," Phys. Rev. 78 [3] 275-289 (1950).

19. J.P. Hirth and J. Lothe, "Theory of Dislocations," John Wiley and Sons, New York (1982).

20. W.E. Tefft, "Elastic Constants of Synthetic Single Crystal Corundum," J. Res. Nat. Bur. Std., 70A [4] 277-80 (1966).

21. J.D. Snow and A.H. Heuer, "Slip Systems in Al_2O_3," J. Am Ceram. Soc. 56 [3] 153-57 (1973).

22. D.P. DiVincenzo and C. Rottmann, "Structure of Asymmetric Small-Angle Grain Boundaries," Phys.Rev B 37 5242-51 (1988).

23. G. Wulff, "Zur Frage der Geschwindigkeit des Wachstums und der Auflösung der Krystallflachen," Z. Krist. 34 449-530 (1901).

24. C. Herring, "The use of Classical Macroscopic Concepts in Surface-Energy Problems," pp. 5-81 in *Structure and Properties of Solid Surfaces*, Robert Gomer and Cyril Stanley Smith eds. The University of Chicago Press, Chicago, IL (1953)

25. W.C. Carter, J.E. Blendell, C.A. Handwerker and J.W. Cahn, to be published.

26. J.W. Cahn and C.A. Handwerker, "Equilibrium Geometries of Anisotropic Surfaces and Interfaces," Mat. Sci. Eng., in press (1993).

27. B.J. Hockey, private communication.

Figure Captions:

1. Experimental configuration to produce sapphire bicrystals with anorthite glass at the interface.

2. Microstructure of sapphire specimens with vitreous grain boundaries; 2h of sintering at 1650°C with 7 MPa compressive stress applied normal to the interface.

3. Sapphire boundary migration as a consequence of heat treatment at 1600°C. (a) 10 hours of annealing; (b) 20 h of annealing; (c) 60 h of annealing. These annealing times are in addition to the 2 h of sintering at 1650°C and 7 MPa normal load.

4. Bicrystal formation; 10 h. at 1600°C with a 10 MPa compressive stress applied normal to the interface.

5. Boundary illustrating the structures observed. Depending on the angle between the interface normal and the mean interface normal (vertical in this figure), the boundary may be: (a) a fully-wetted, faceted solid liquid interface; (b) a low-angle grain boundary; or (c) a mixture of the two.

6. Fully-wetted boundaries between the two sapphire crystals. (a) extremes of structure; (b) boundary with very little glass at the interface.

7. Low-angle grain boundary consisting of individual dislocations.

8. Partially-wetted boundaries between the two sapphire crystals. (a) glass pockets, g, are bounded by (0001) and (1$\bar{2}$13) planes. The glass pockets are connected by a low-angle grain boundary; (b) partially-wetted boundary with very little glass at the boundary.

9. Energy of a low-angle grain boundary from the Reed-Shockley equation; $\gamma_{gb} = \gamma_{gb}^{\circ}(\Phi)\cdot\Theta\cdot[A(\Phi) - \ln\Theta]$. The energy is more sensitive to misorientation, Θ, between crystals than to the angle of the grain boundary normal, Φ.

10. Wulff shape for sapphire assuming only (0001) and (1$\bar{2}$13) planes in the crystal. (a) Surface energy circle for a faceted surface consisting of (0001) and (1$\bar{2}$13) facets. The distance from the origin to the circle is the surface energy of the surface with a unit vector normal $\mathbf{n}$. The vector from the origin to the corner defines the diameter of the surface energy circle such that the surface energy, γ, is given by $\gamma = \mathbf{n}\cdot\boldsymbol{\sigma}$. (b) The outer envelop of such circles defines the surface energy curve. This curve is made up of six circles, one for each corner of the figure.

11. Wetted bicrystal boundary energy is determined from the two surface energy curves, tilted relative to each other. The energy of the wetted boundary is obtained by adding the energies of the two solid-liquid interfaces as a function of the angle, Φ.

12. Surface energy as a function of orientation for a wetted, faceted bicrystal boundary. Also shown inside the surface energy curve is the Wulff shape constructed from this surface energy curve. For any angle, Φ, the distance from the origin to the curve gives the surface energy for the wetted bicrystal. The 12 local minima in the surface energy curve correspond to distinct morphologies of the wetted boundaries. At $\pm 3.5°$ the boundary consists of a flat basal surface facing a faceted basal and pyramidal surface. At 57.5°, the interface consists of a flat pyramidal, and a faceted pyramidal and basal surface. At 64.5° (not shown) the surface consists of a flat pyramidal and a faceted surface consisting of pyramidal planes.

13. (a) Comparison of a low-angle grain boundary Wulff shape (large circle) with the Wulff shape of a wetted, faceted bicrystal boundary. The two figures are scaled so that the grain boundary Wulff shape intersects the bicrystal Wulff shape at 38°. The inner envelope of the two overlaid Wulff shapes, (b), is the Wulff shape of the interface. Between angles of 3.5° and 38°, the lowest energy is obtained for a partially-wetted interface. The energy of the interface is shown in (c).

A1. Schematic of the addition of the diameter vectors from the rotated single crystal Wulff shapes to obtain the combined Wulff shape. The vectors from the origin of the combined Wulff shape to the corners define diameter vectors for the bicrystal surface energy curve.

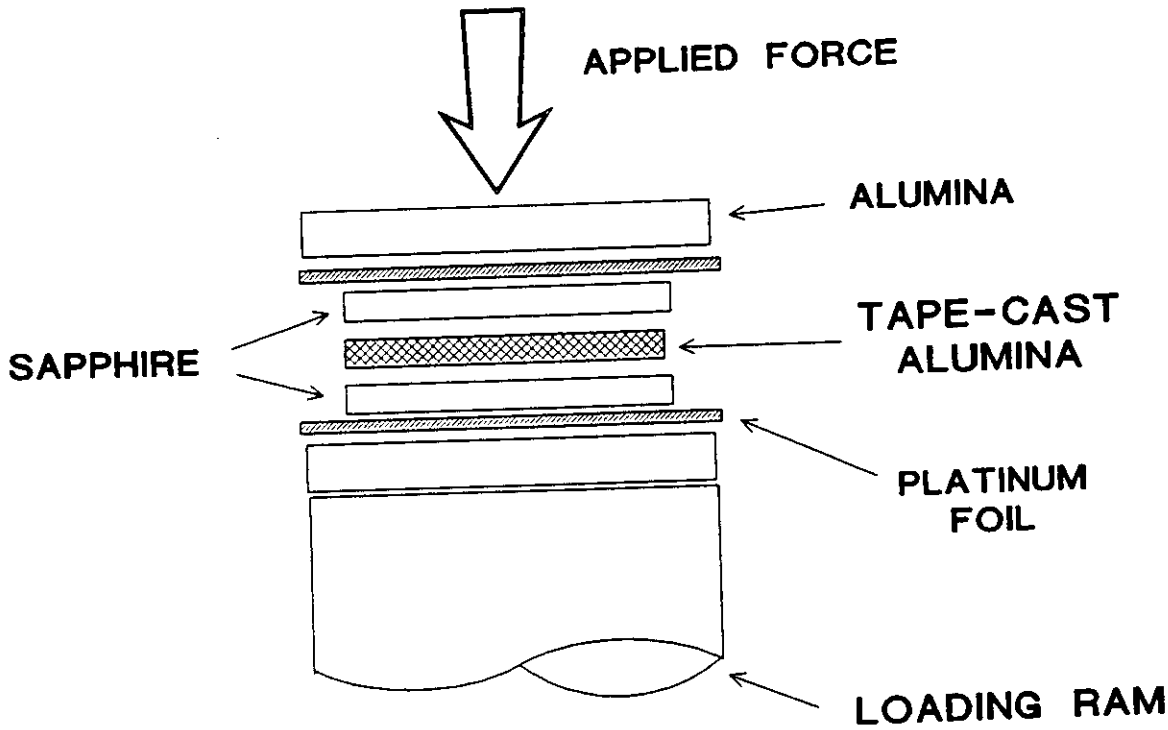

1. Experimental configuration to produce sapphire bicrystals with anorthite glass at the interface.

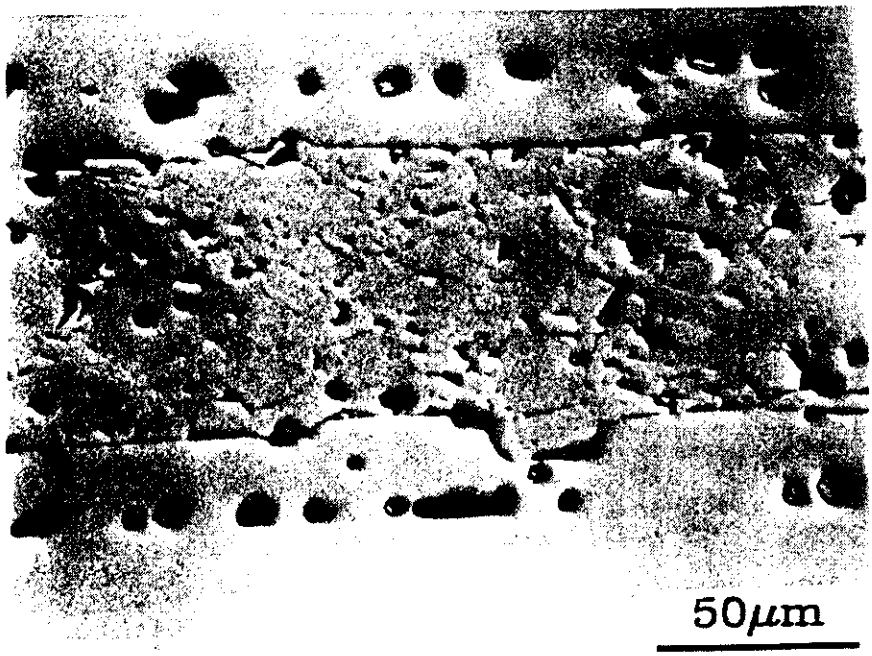

2. Microstructure of sapphire specimens with vitreous grain boundaries; 2h of sintering at 1650°C with 7 MPa compressive stress applied normal to the interface.

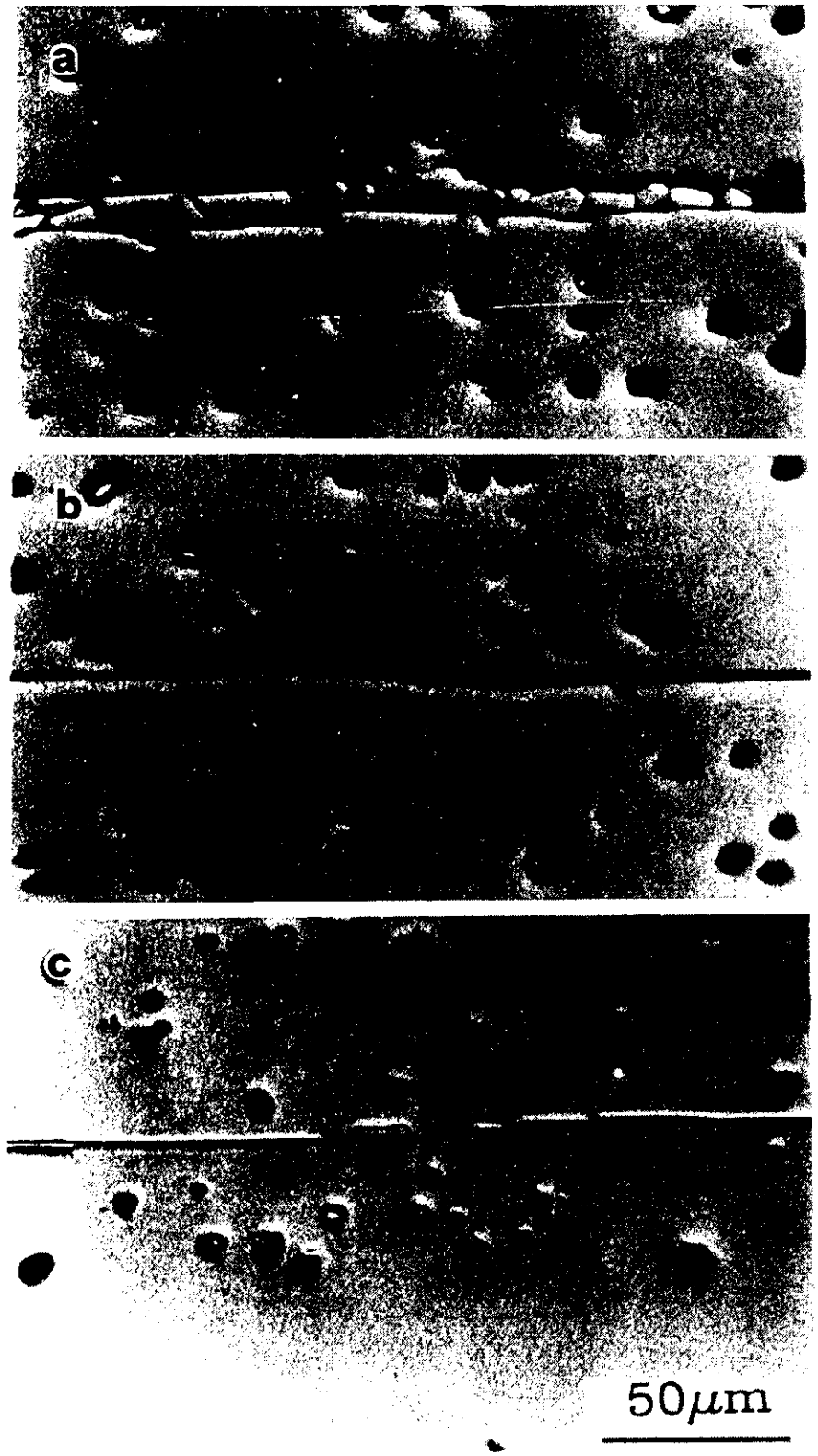

3. Sapphire boundary migration as a consequence of heat treatment at 1600°C. (a) 10 hours of annealing; (b) 20 h of annealing; (c) 60 h of annealing. These annealing times are in addition to the 2 h of sintering at 1650°C and 7 MPa normal load.

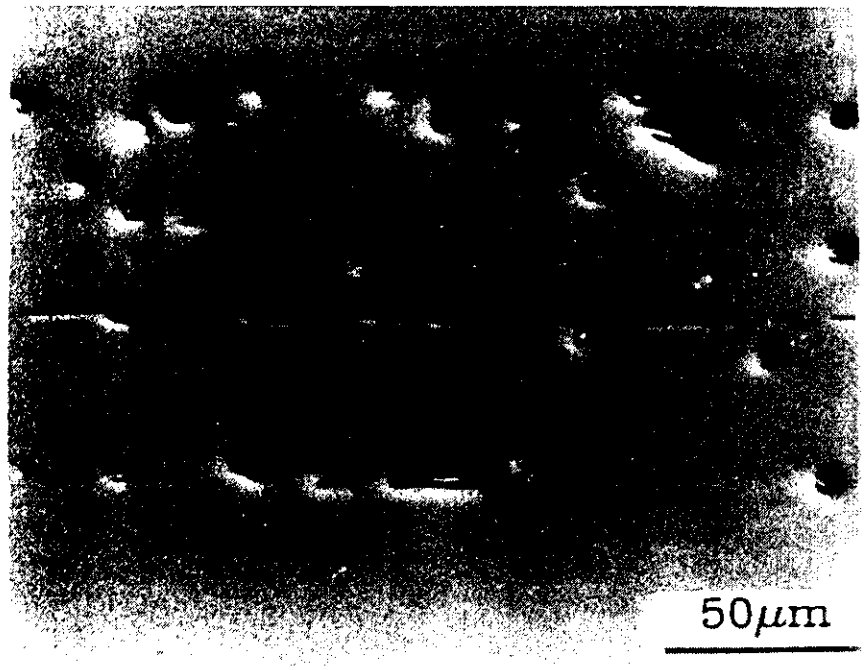

4. Bicrystal formation; 10 h. at 1600°C with a 10 MPa compressive stress applied normal to the interface.

5. Boundary illustrating the structures observed. Depending on the angle between the interface normal and the mean interface normal (vertical in this figure), the boundary may be: (a) a fully-wetted, facetted solid liquid interface; (b) a low-angle grain boundary; or (c) a mixture of the two.

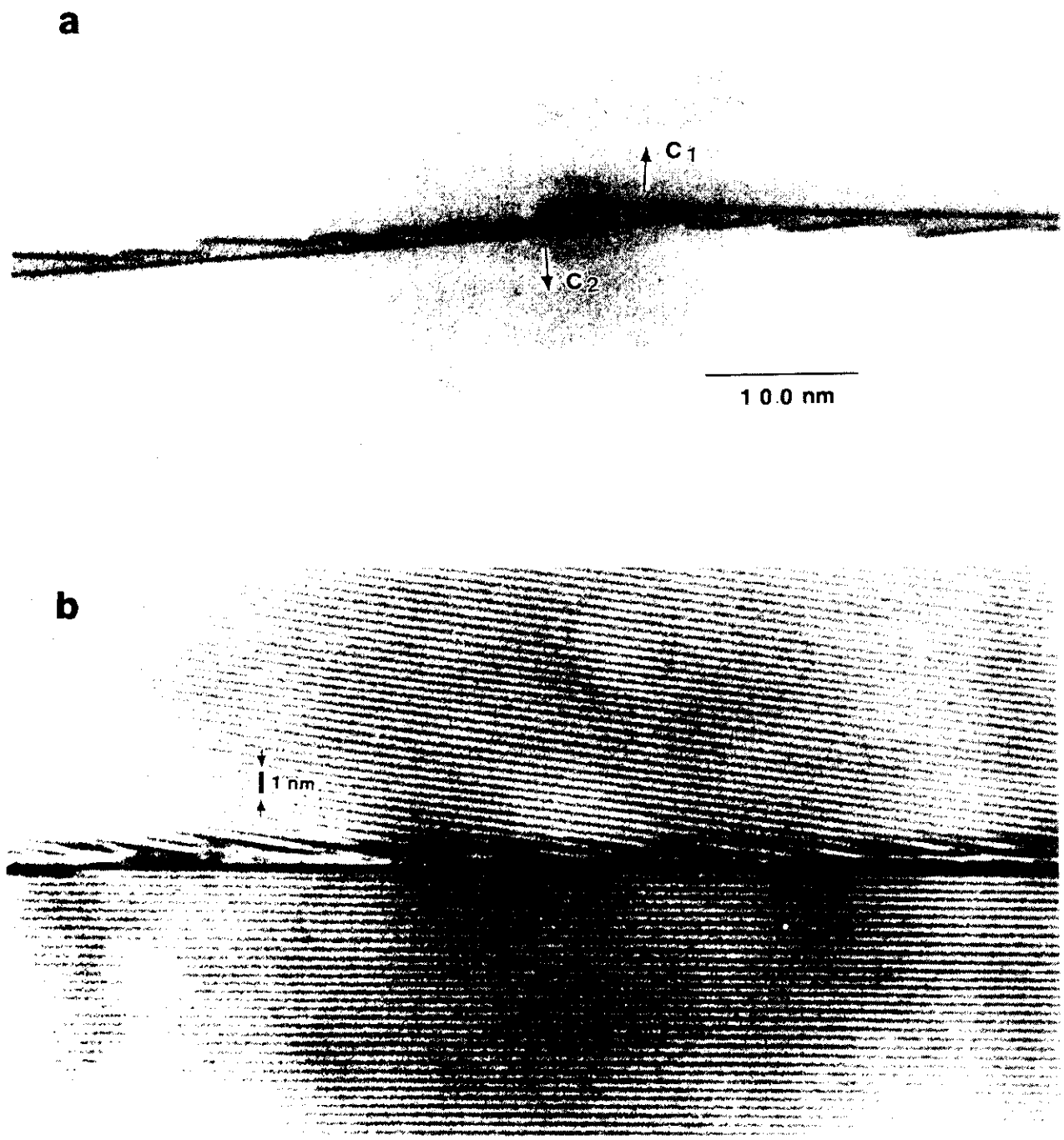

6. Fully-wetted boundaries between the two sapphire crystals. (a) extremes of structure; (b) boundary with very little glass at the interface.

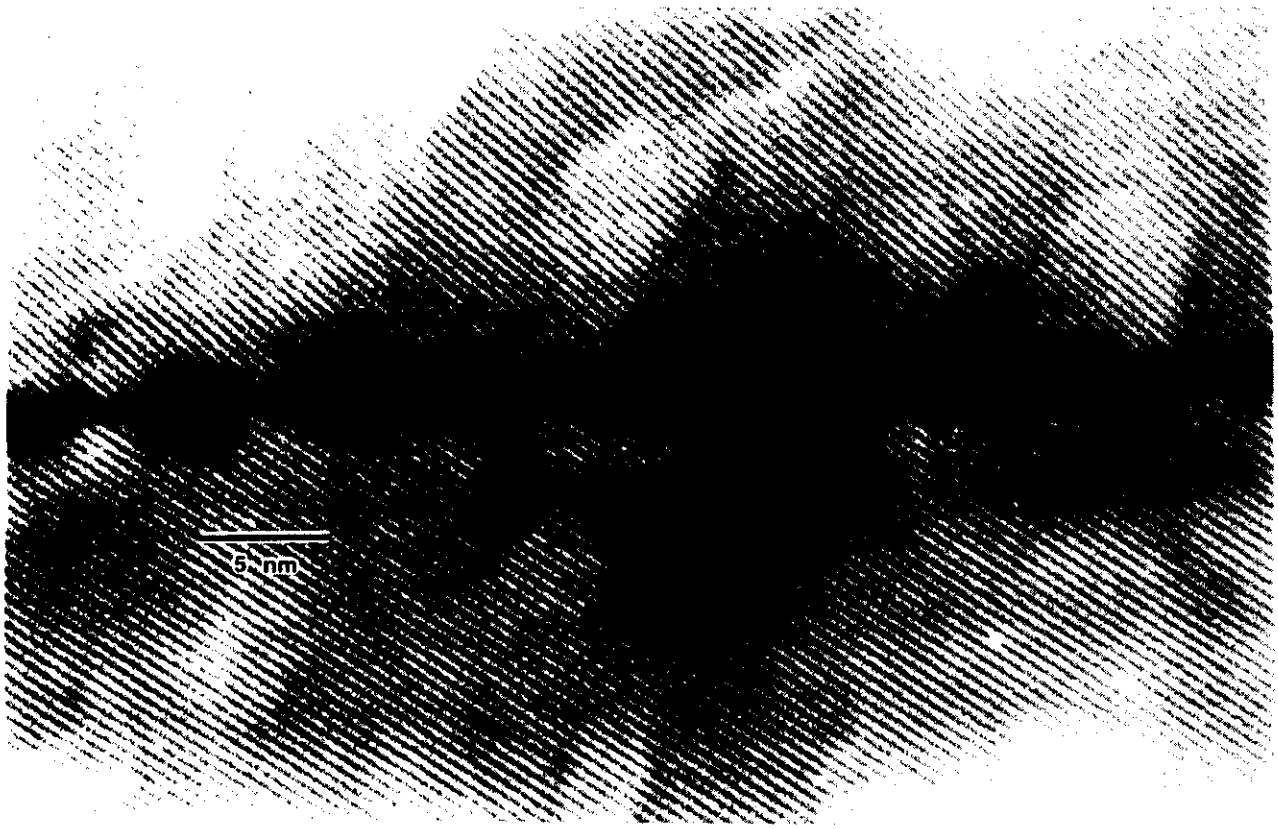

7. Low-angle grain boundary consisting of individual dislocations.

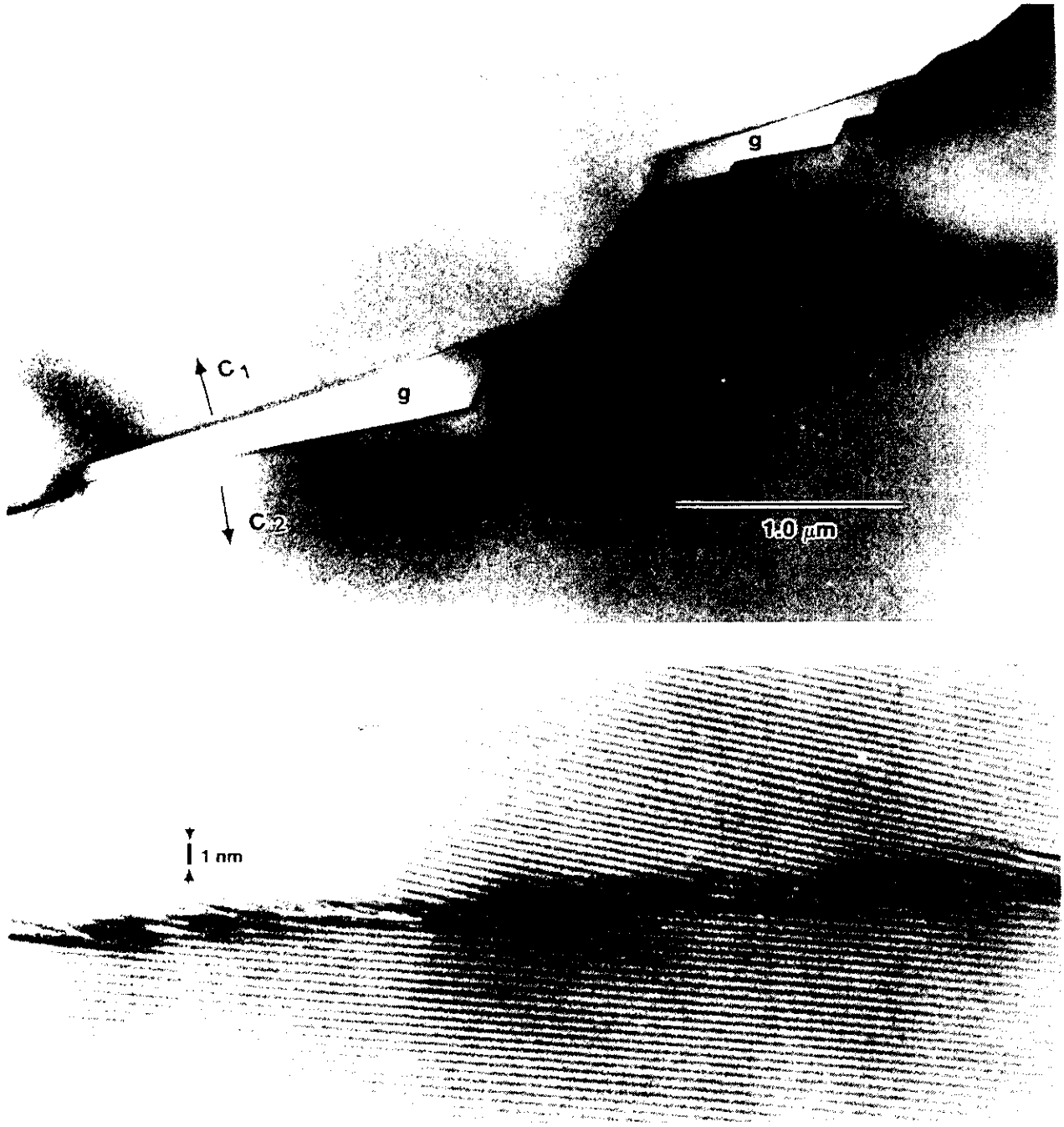

8. Partially-wetted boundaries between the two sapphire crystals. (a) glass pockets, g, are bounded by (0001) and (1$\bar{2}$13) planes. The glass pockets are connected by a low-angle grain boundary; (b) partially-wetted boundary with very little glass at the boundary.

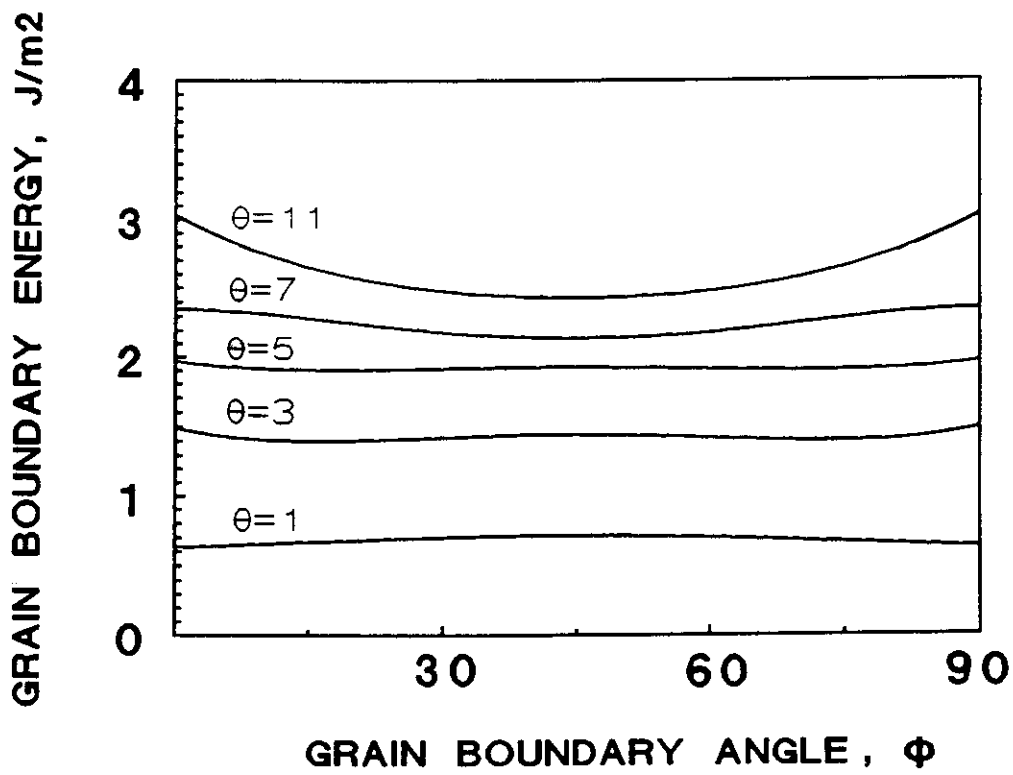

9. Energy of a low-angle grain boundary from the Reed-Shockley equation; $\gamma_{gb} = \gamma_{gb}^{o}(\Phi) \cdot \Theta \cdot [A(\Phi) - \ln \Theta]$. The energy is more sensitive to misorientation, Θ, between crystals than to the angle of the grain boundary normal, Φ.

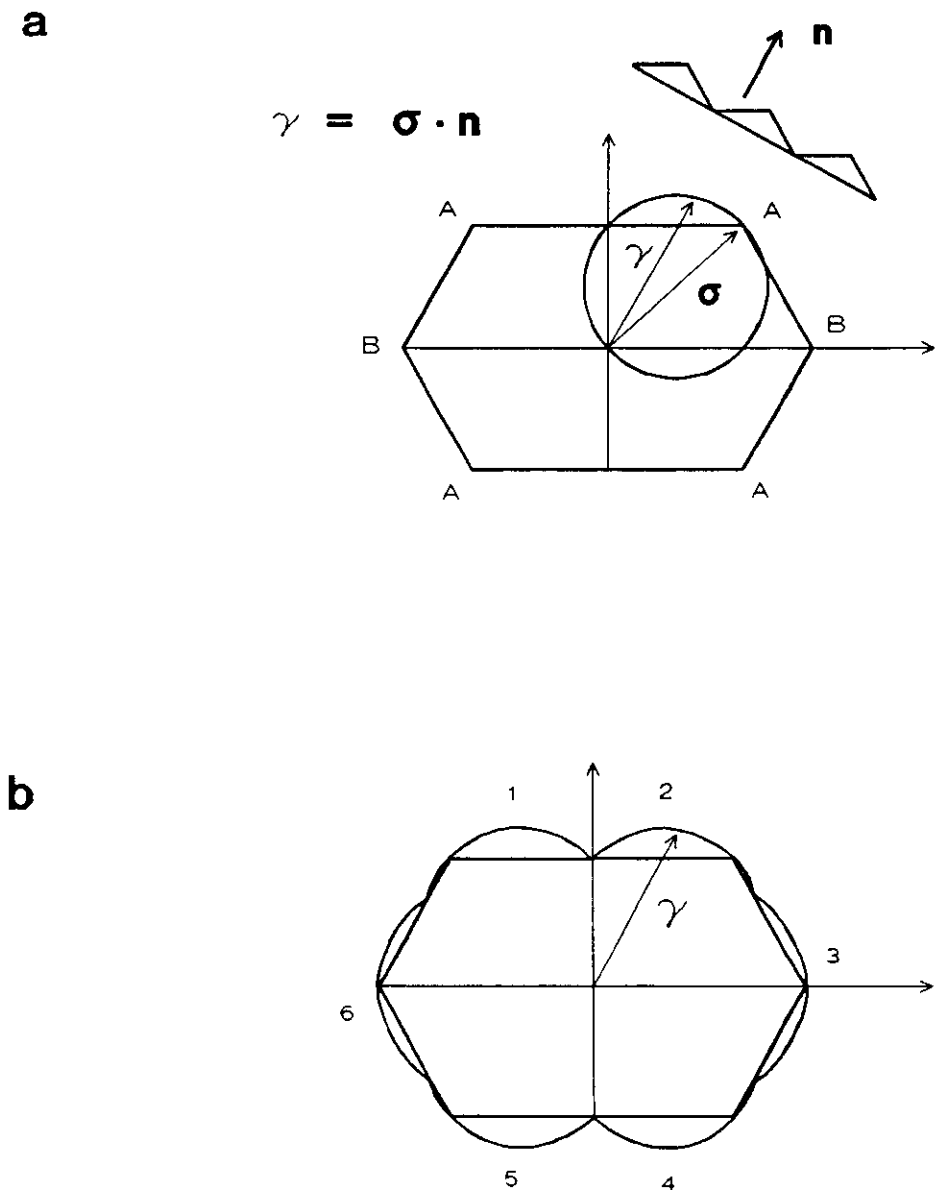

10. Wulff shape for sapphire assuming only (0001) and (1$\bar{2}$13) planes in the crystal. (a) Surface energy circle for a facetted surface consisting of (0001) and (1$\bar{2}$13) facets. The distance from the origin to the circle is the surface energy of the surface with a unit vector normal **n**. The vector from the origin to the corner defines the diameter of the surface energy circle such that the surface energy, γ, is given by $\gamma = \mathbf{n} \cdot \sigma$. (b) The outer envelop of such circles defines the surface energy curve. This curve is made up of six circles, one for each corner of the figure.

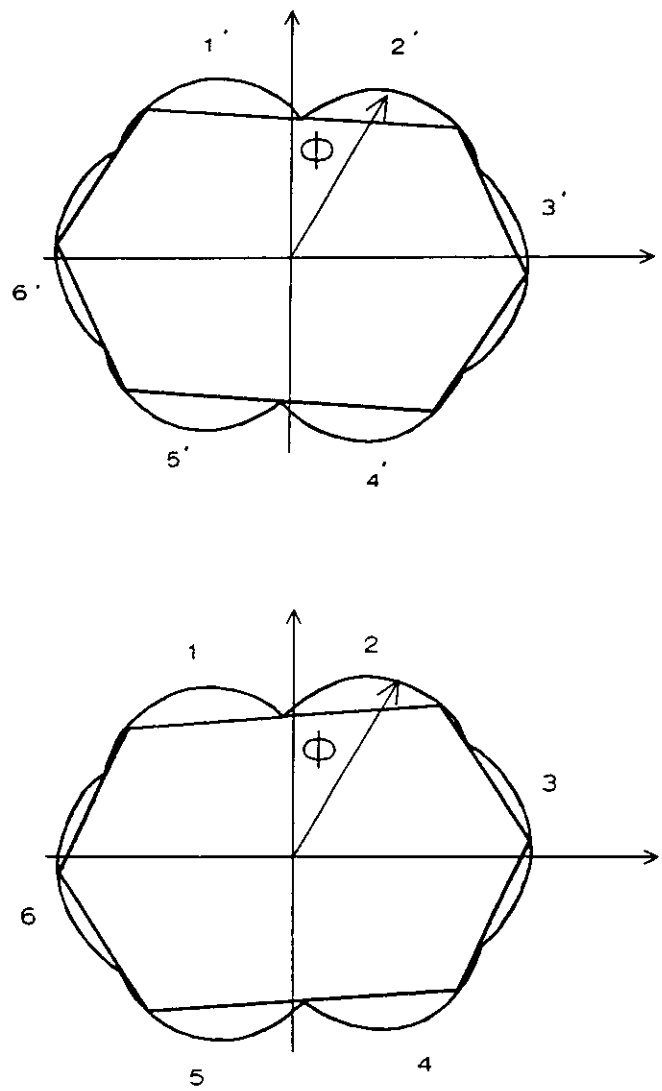

11. Wetted bicrystal boundary energy is determined from the two surface energy curves, tilted relative to each other. The energy of the wetted boundary is obtained by adding the energies of the two solid-liquid interfaces as a function of the angle, Φ.

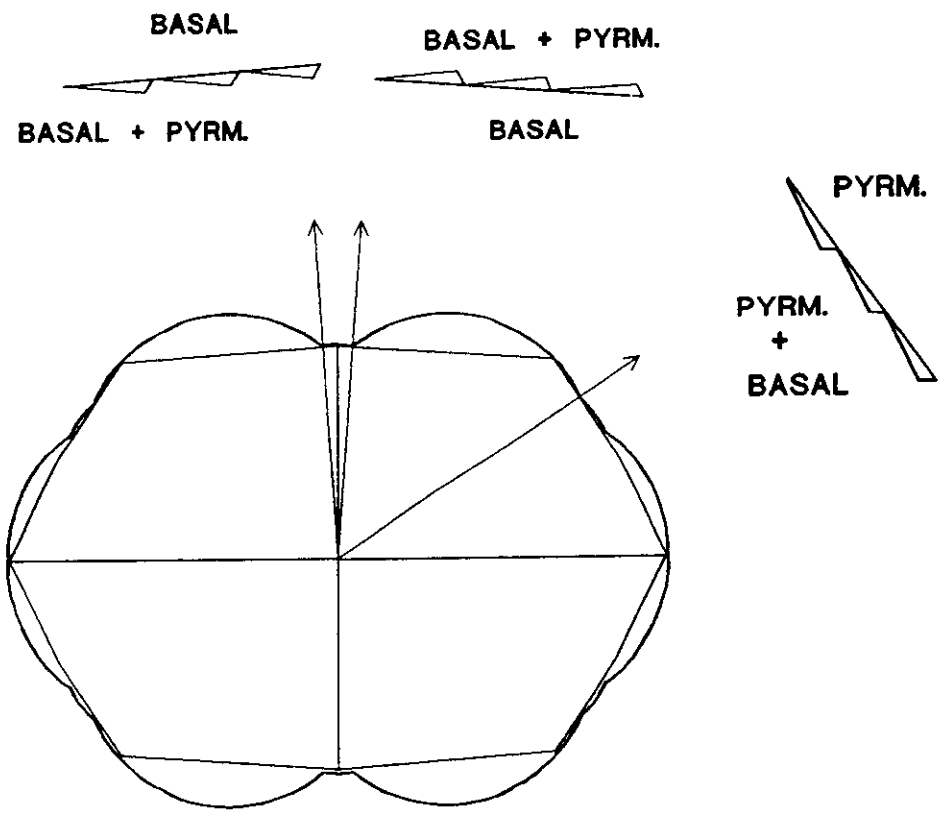

12. Surface energy as a function of orientation for a wetted, facetted bicrystal boundary. Also shown inside the surface energy curve is the Wulff shape constructed from this surface energy curve. For any angle, Φ, the distance from the origin to the curve gives the surface energy for the wetted bicrystal. The 12 local minima in the surface energy curve correspond to distinct morphologies of the wetted boundaries. At ±3.5° the boundary consists of a flat basal surface facing a facetted basal and pyramidal surface. At 57.5°, the interface consists of a flat pyramidal, and a facetted pyramidal and basal surface. At 64.5° (not shown) the surface consists of a flat pyramidal and a facetted surface consisting of pyramidal planes.

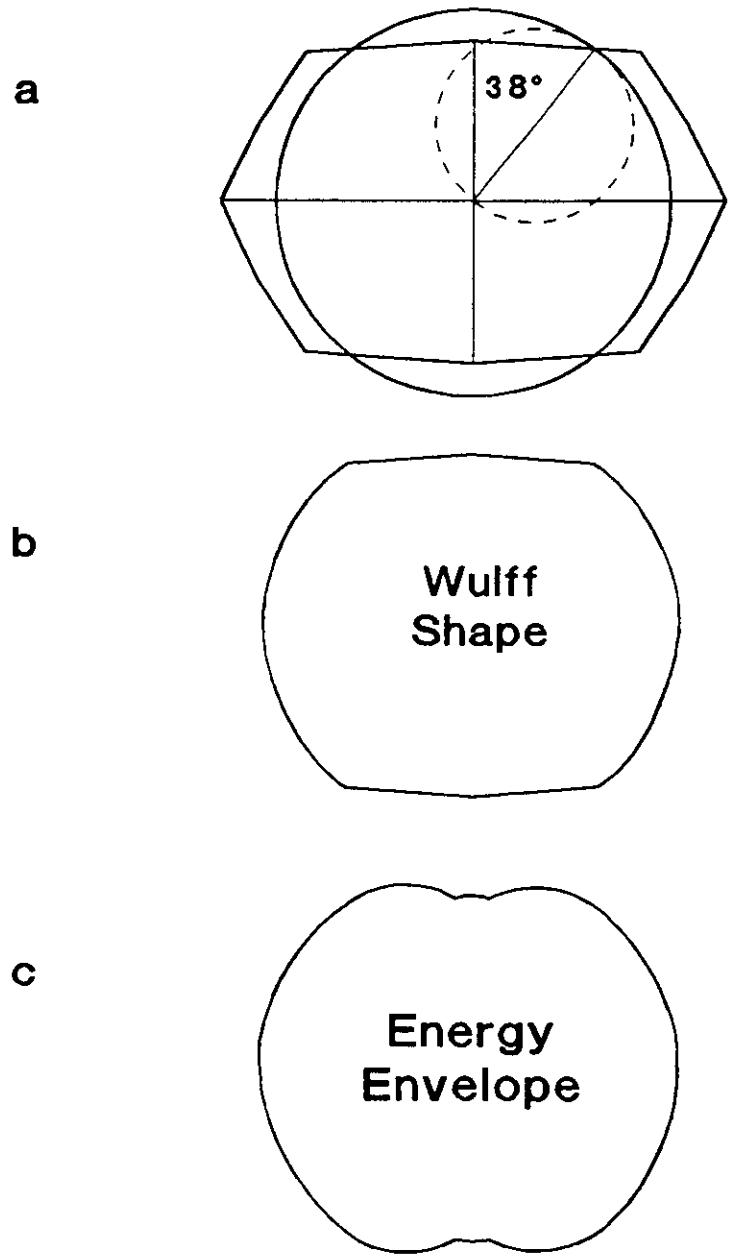

13. (a) Comparison of a low-angle grain boundary Wulff shape (large circle) with the Wulff shape of a wetted, facetted bicrystal boundary. The two figures are scaled so that the grain boundary Wulff shape intersects the bicrystal Wulff shape at 38°. The inner envelope of the two overlaid Wulff shapes, (b), is the Wulff shape of the interface. Between angles of 3.5° and 38°, the lowest energy is obtained for a partially-wetted interface. The energy of the interface is shown in (c).

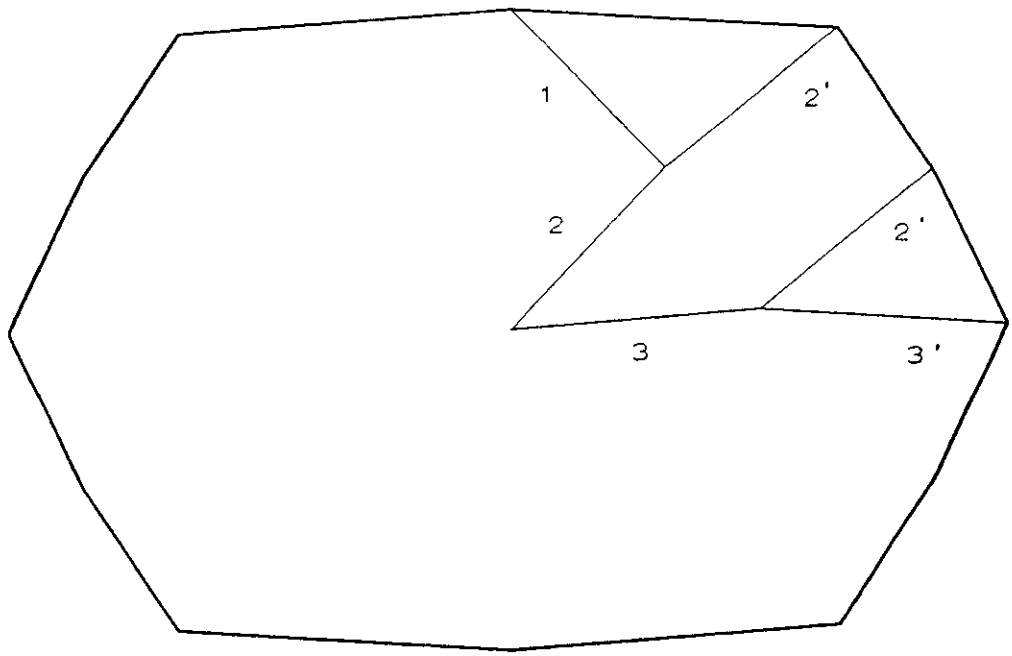

A1. Surface energy as a function of orientation for a wetted, facetted bicrystal boundary. Also shown inside the surface energy curve is the Wulff shape constructed from this surface energy curve. For any angle, Φ, the distance from the origin to the curve gives the surface energy for the wetted bicrystal. The 12 local minima in the surface energy curve correspond to distinct morphologies of the wetted boundaries. At ±3.5° the boundary consists of a flat basal surface facing a facetted basal and pyramidal surface. At 57.5°, the interface consists of : flat pyramidal, and a facetted pyramidal and basal surface. At 64.5° (not shown) the surface consists of a flat pyramidal and a facetted surface consisting of pyramidal planes.